Investigating the role of Large Igneous Provinces (LIPs) in the Mid-Cenomanian Event (MCE): Nd, Sr, and Os isotope evidence from the Iona-1 core

---

A Senior Honors Thesis Presented to

the Faculty of the Department of Earth and Atmospheric Sciences

University of Houston

In Partial Fulfillment

of the Requirements for the Degree

Bachelor of Science

By

Olivia Wren

April 2020

Abstract

Based on Earth's climate cycling history of icehouse to greenhouse states and isotopic proxies for paleoclimate and environmental conditions, there is a direct relationship between volcanism, weathering, ocean circulation, and the carbon perturbations that define these cycles. Ocean anoxic events (OAEs) occur during Earth's greenhouse states. The OAEs are defined as periods of increased oxygen depletion (anoxia) in the global ocean and are identified in lithostratigraphy as globally traced units of black shale. While geochemical constraints of ocean anoxia are well documented, the biogeochemical triggers of these anoxic events are not well understood. It is theorized that the Cenomanian-Turonian Ocean Anoxic Event 2 (OAE2; ca 94 Ma) was at least partly triggered by the emplacement of a large igneous province (LIP) based on Nd isotope data indicating enhanced nutrient content in seawater from increased hydrothermal activity (Eldrett et al., 2014; Jenkyns et al., 2010). The Mid-Cenomanian OAE (MCE; ca 96.5 Ma) may have been a prelude to OAE2 (Coccioni and Galotti, 2003). Understanding the paleoclimate of the MCE would contribute to a better understanding of OAE2 and how OAEs may be related. However, there is scarce evidence for the MCE's environmental conditions. This study reconstructs the mid-Cenomanian Cretaceous Western Interior Seaway (KWIS) seawater ε Nd, $^{87}Sr/^{86}Sr$ and $^{187}Os/^{188}Os$ from Shell's Iona-1 research core of southwest Texas to test the role of changes in ocean circulation and the emplacement of a LIP in triggering the MCE. The modern ocean ranges in ε Nd values of -14.34 ± 0.13 to -8.0 ± 0.3 (Flierdt et al., 2016). The MCE data from this study show a positive ε Nd excursion (-4.14 to -0.56) likely as a result of a highly radiogenic ε Nd input from submarine volcanism. The emplacement of the Caribbean large igneous province (CLIP; 98.7 Ma) was carried northward into the KWIS by the migration

of the equatorial Atlantic Tethyan water mass during the early Cenomanian (Serrano et al., 2011; Eldrett et al., 2017). This northward migration of the Tethyan water mass with high nutrient contents from volcanic input may explain the positive ε Nd excursion and contribute to the onset of ocean anoxia observed in the MCE.

Contents

Figures

Tables

1. Introduction

Ocean anoxic events (OAEs) represent large perturbations in the global carbon cycle and are recorded in stratigraphy as globally traced units of organic-rich black shales (Jenkyns, 2010). The MCE was a relatively short-term occurrence (400 ky) (Coccioni and Galeotti, 2003). Its impact on the carbon cycle and the biotic record requires further investigation as it has been described as a prelude to OAE2 (Coccioni and Galeotti, 2003). Isotope data obtained from shales deposited during this time provide insight into the climate system during ocean anoxia. Neodymium (Nd) isotopes have been used to reconstruct ancient ocean circulation patterns, which may be used to understand the relationships between water mass movement, ocean anoxia, and climate (Martin et al., 2012). Strontium (Sr) isotope values and excursions provide a proxy for distinguishing crustal and mantle sources of nutrient inputs into seawater (Jones and Jenkyns, 2001). Research of ancient ocean anoxia is important in understanding the expansion of anoxic water masses present in the oceans today, as well as their relationship to the modern climate and the current state of climate change (Jenkyns, 2010).

OAEs have occurred throughout the geologic past lasting from 250,000 to one million years and represent some of the largest biogeochemical and climatic perturbations in Earth's history as they are understood to be a consequence of a warming climate and a rapid increase in greenhouse gasses in the atmosphere (Jenkyns, 2010). As the global climate warms, nutrient discharge to the ocean surface increases (Jenkyns, 2010). Greater availability of nutrients results in an increase in the flux of organic matter in the ocean basin (Jenkyns, 2010). The rapid growth in organic matter is followed by an influx of CO_2 and consumption of all dissolved oxygen by organisms, resulting in ocean anoxia (Jenkyns, 2010). Ocean anoxia is accompanied by

continued climate warming, eustatic sea-level rise and epicontinental sea development (Friedrich et al., 2009). Chemostratigraphic identification of OAEs includes positive carbon isotope excursions due to the extensive removal of ^{12}C by rapid burial of organic carbon (Corg) (Eldrett et al., 2015). Additional isotopes such as Nd, and Sr have been utilized as proxies to better reconstruct the paleoclimate and environmental processes.

The mechanisms to produce such biogeochemical changes in the oceans are not well constrained, and further investigation is needed to understand the driving mechanisms leading to these global periods of anoxia. Thus, OAE research is directed at understanding the precursing climatic events that preconditioned anoxic conditions, and especially the main trigger of an OAE itself. Possible triggers of OAEs are associated with enhanced nutrient discharge in oceans by increased continental weathering, changes in ocean circulation concerning warm bottom waters, and increased hydrothermal input from submarine volcanism (Martin et al., 2012). It is important to note that conflicting data have been published regarding the trigger(s) responsible for ocean anoxia and continued research is required.

The MCE (96.5 Ma) is one of the least studied OAEs. Yet, it has been described as a prelude to OAE2, a well studied and documented OAE due to its globally traced black shale beds and destructive paleoenvironmental impact (Coccioni and Galeotti, 2003). Therefore, understanding the biogeochemical processes that led to the occurrence of the MCE would provide insight into the driving mechanisms of OAE2. The most commonly used method in understanding the biogeochemical processes that lead to OAEs is to obtain chemical signatures from isotopes in ancient marine carbonate deposits (Jenkyns, 2010). In this study, the first reconstruction of KWIS seawater εNd and $^{87}Sr/^{86}Sr$ from shale samples of Shell's Iona-1 research

core derived from the Eagle Ford Group (Figure 1) is presented. These new data are used as environmental proxies to constrain the biogeochemical perturbations of ocean anoxia throughout the MCE.

1.1 Neodymium Isotopes in Black Shales

The distribution of Nd isotopes within seawater is controlled by inputs of weathered continental material as well as submarine magmatic activity (Zheng et al., 2013). Therefore, Nd isotopes are used as environmental proxies for weathering, submarine volcanism and ancient ocean circulation reconstruction (MacLeod et al., 2008). Seawater $^{143}Nd/^{144}Nd$ expressed as ε Nd is especially useful in examining OAEs because it provides a proxy that is independent of the carbon cycle and is reliable for use in reconstructing ancient ocean circulation patterns (Abbott et al., 2016). Additionally, Nd isotopes have been used as a proxy for eustatic changes (Wendler et al., 2016). This is important in correlating eustatic sea-level rise with greenhouse climate conditions and ocean anoxia. However, this signal may be influenced by the effects of a rapidly changing climate and inputs of continental weathering (Wright et al., 2017). Seawater ε Nd acts as a tracer for large water masses, and is useful in the reconstruction of Cretaceous ocean circulation (Moiroud et al., 2016). The ocean residence time of Nd of 300 to 600 years is much shorter than the ocean mixing time of 1,500 years (Moiroud et al., 2016). Therefore, positive and negative ε Nd excursions signify the movement of bottom water masses over the seafloor (Moiroud et al., 2016).

Neodymium isotopes have also been used as an environmental proxy for increased hydrothermal activity on the seafloor (Zhend et al., 2013). Mid-ocean ridge (MOR) basalt has notably high radiogenic ε Nd values of approximately +10 (Zheng et al. 2013). A sudden

positive ε Nd excursion may indicate intensified hydrothermal activity from increased ocean crust production at MORs, or the emplacement of LIPs.

1.2 Strontium Isotopes in Black Shales

The $^{87}Sr/^{86}Sr$ ratios in marine sedimentary rocks record perturbations of the global carbon cycle. The $^{87}Sr/^{86}Sr$ ratios in carbonates and their resulting shifts from radiogenic to non-radiogenic values provide proxies for continental weathering and hydrothermal activity (Jones and Jenkyns, 2001). Amplified hydrothermal activity, notably from increased ocean-crust production at MORs and LIPs, may produce up to gigatons of CO_2 outgassing and can contribute to global warming (Jones and Jenkyns 2001). The increased hydrothermal input increases nutrient addition and surface water biological production, preconditioning factors to ocean anoxia (Jones and Jenkyns 2001). Increased hydrothermal activity is identified in seawater as an excursion to lower $^{87}Sr/^{86}Sr$ ratios (Jones and Jenkyns 2001). A positive $^{87}Sr/^{86}Sr$ excursion to more radiogenic values is interpreted to be a result of increased continental crustal runoff into the global ocean as a consequence of amplified weathering (Blättler et al., 2011).

1.3 Ocean Circulation and OAEs

The reconstruction of paleocirculation patterns during periods of anoxia provides insight into changes in paleoclimate (Zheng et al., 2013). Ocean circulation plays a key role in global heat transport and nutrient delivery, therefore changes in ocean circulation are associated with changes in climate conditions (Zheng et al., 2014). For example, the acceleration of the hydrological cycle is accompanied by global warming (Martin et al., 2012). Changes in circulation patterns impact both climate and carbon cycling (Martin et al., 2012). If changes in ocean circulation patterns result in higher nutrient concentrations and promote surface

productivity, then changing circulation may trigger ocean anoxia (MacLeod et al., 2008). The reconstruction of ocean circulation is based on understanding that water masses are marked by signature Nd isotopes from surrounding continental plates (Zheng et al., 2013). These Nd isotope signatures remain constant during circulation and allow for the tracing of water masses (Zheng et al., 2013).

1.4 Large Igneous Provinces and OAEs

Large igneous provinces do not originate from traditional tectonic-related seafloor spreading. The LIPs are a result of mantle plumes that produce magmas that make submarine flood basalts and ocean plateaus (Snow et al., 2005). The associated eruptions may only last days to decades, however, the erupted volcanic gasses and magmas are explosive, destructive and occur in massive volumes (Coffin and Eldholm, 1994). Neodymium and Os are commonly used as environmental proxies to trace LIP involvement in global carbon perturbations such as OAEs. Positive ε Nd excursions are either the result of terrigenous volcanic debris runoff or the emplacement of LIPs as discussed previously. The $^{187}Os/^{188}Os$ ratios of marine sediments records a negative excursion in chemostratigraphy as a result of LIP involvement.

Both the High Arctic LIP (HALIP) and the Caribbean LIP (CLIP) (Figure 2) have been proposed as triggers responsible for the onset of OAE2 (Deegan et al., 2016; Snow et al., 2005). However, due to the lack of accurate geochronology for both the HALIP and the CLIP, there is uncertainty in the timing of the emplacement of each LIP and the duration of associated eruptions. The timing of LIP eruptions has been constrained by ^{40}Ar -^{39}Ar analysis of basalts. Published data show a variety of dates. For example, the HALIP eruptions have been dated to range from 130-120 Ma (Deegan et al., 2016), and 93-60 Ma (Schroder et al., 2019). This

inconsistency in the dates of LIP activity creates a challenge in concluding LIP involvement with the onset of an OAE.

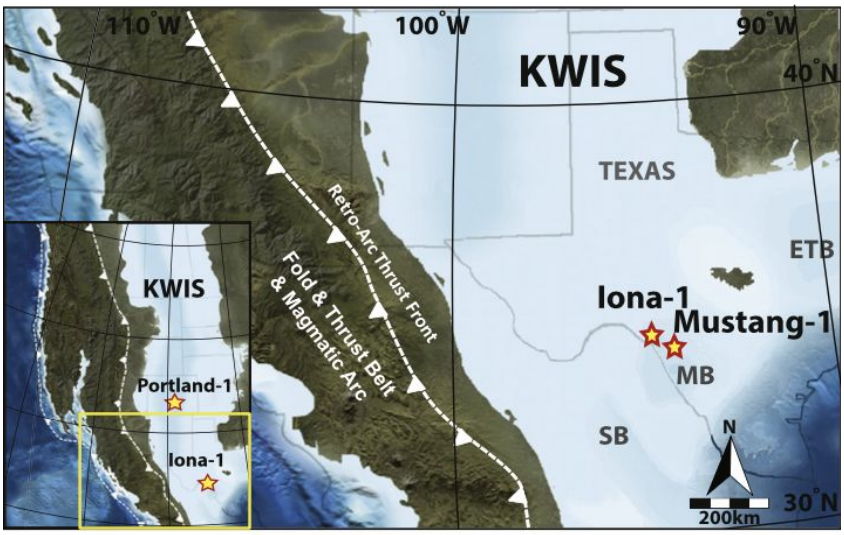

Figure 1: Star indicating the Iona-1 core location during the mid-Cenomanian (Eldrett et al., 2015).

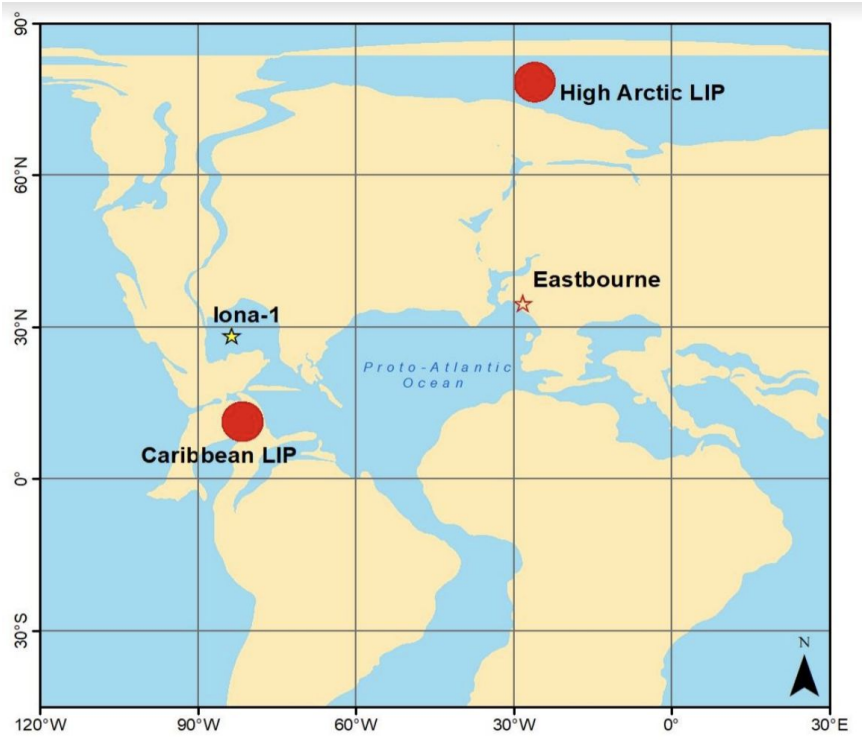

Figure 2: Map showing a paleogeographic reconstruction of the Proto-Atlantic Ocean and surroundings ca 96.5 Ma. The approximate locations of the Caribbean Large Igneous Province, High Arctic Large Igneous

Province, Iona-1 core and Eastbourne section are indicated. (map modified by Lauker (2018) from http://www.odsn.de/odsn/services/paleomap/paleomap.html)

2. Materials and Methods

2.1 The Iona-1 Core

Samples used in this study consist of organic-rich marls and carbonates from Shell's Iona-1 research core drilled at 29 13.510N, 100 44.490W from the Eagle Ford Group in West Texas (Figure 1). The Eagle Ford group was deposited under the KWIS from 98 to 90 Ma within the Cenomanian to Turonian (Minisini et al., 2018). The core encompasses marine sediments of the MCE as well as OAE2 (Eldrett et al., 2017). Litho- and chemo- stratigraphic analysis of the Iona-1 core by Eldrett et al. (2014) identified the MCE as a 5 meter long section of mudstone with high organic matter content, and a characteristic double-peak δ 13C excursion. The analysis of the Eagle Ford group indicates that the MCE portion of the Iona-1 core was deposited distally (>500 km) from the shoreline, in a sediment-starved foreland basin in relatively shallow waters (30 m) during a period of long-term KWIS transgression and local tectonic inactivity (Eldrett et al. 2017). These environmental conditions made for the ideal conditions for successful mudstone deposition (Minisini et al., 2018). The Iona-1 core sample contain two positive δ^{13}Corg excursions as well as high total organic carbon (TOC) during the MCE (Eldrett et al., 2017).

2.2. Sample decomposition for Nd and Sr

Eighteen samples were hand crushed and processed for high-precision $^{143}Nd/^{144}Nd$ and $^{87}Sr/^{86}Sr$ analysis. From 0.2 to 0.5 gram of each sample was weighed and added to clean 50ml teflon beakers, followed by 5ml of ammonium acetate solution for cation exchange. All samples were leached to remove the clay components of the samples through ion exchange, leaving only

the carbonate component. After 12 hours, the acetate was decanted and the samples were rinsed three times with 18.2Ω Millipore water. The samples were then dissolved in about 2ml 1N acetic acid for about 1 hour. The samples were centrifuged, and the supernatant was carefully decanted into teflon beakers and dried. The samples were then redissolved in a few ml of 6 N HNO3 and refluxed overnight to convert the acetate to nitrate form. The residues were dissolved in 0.5N HNO3 and transferred to new, pre-weighed, acid-cleaned 50 ml centrifuge tubes. Five ml solutions were aliquoted for elemental analysis at the University of Houston ICP analytical lab for determination of the major and trace element concentrations. Aliquots with a total of 200 ng of Nd were taken for high precision $^{143}Nd/^{144}Nd$ analysis and 300 ng of Sr for $^{87}Sr/^{86}Sr$ analysis.

2.3 Sm - Nd separation and TIMS analysis

A mixed ^{150}Nd-^{148}Sm spike was added to the Nd aliquots for obtaining Sm and Nd concentrations. Fractions containing approximately 200 ng of Nd were purified using an LN spec column. All 18 samples processed for Nd and two blanks (spike with no dissolved rock sample) underwent cation column chemistry using various molarities of HCL to isolate rare earth elements (REEs). The collected REE samples were dissolved in a weak acid (0.16N HCL) and passed through LN-spec resin to separate Nd and Sm. Purified solutions of Sm and Nd were collected and dried slowly at 30℃ for 36 hours.

The purified Nd and Sm fractions were dissolved in 1.5 μL of 2N HCL and loaded onto degassed double Re-filaments. The double Re-filament consists of two filaments, one for ionization and one for evaporation. The evaporation filament receives the sample load. Before loading the sample, the filament surface is prepared with a 1.5 μL of 0.7M H_3PO_4 activator. The Nd isotope measurements were carried out on a Thermo Fisher Triton Plus thermal ionization

mass spectrometer (TIMS) at the Radiogenic Isotope Laboratory in the University of Houston (UH). Isotope analysis included the use of a 3 line multi-static technique adapted from a method for high precision Nd isotope analyses (McLeod et al., 2014). Spiked aliquots were measured on the TIMS with beam intensities of 0.2-0.5 V over 180-360 cycles. Nd isotope compositions were corrected for mass fractionation using the exponential law with $^{143}Nd/^{144}Nd = 0.7219$.

2.4 Sr isolation and TIMS analysis

The 18 samples and 2 blanks processed for Sr were passed through Sr Spec resin columns to isolate the Sr fractions. The samples were collected and dried slowly to prepare for filament loading and TIMS analysis. Dried samples were dissolved in 3 μL of concentrated HNO3, and 1.2 μL of the dissolved sample was loaded onto a single degassed Re-filament with TaF_5 and H_3PO_4. Strontium isotope measurements were carried out at the Radiogenic Isotope Laboratory at UH using a Thermo Fisher Triton Plus TIMS. Based on replicate measurements of the SRM 987 Sr standard, the external precision on the $^{87}Sr/^{86}Sr$ ratios is $\leq \pm 5$ ppm (2σ).

3. Results

Trace metals and REEs were measured by Laukner (2018) using an Agilent 8900 QQQ ICP-MS at the University of Houston**.** Calculated element concentrations of trace metals and REEs are presented in table 1. The Sm, Nd and Sr abundances in table 1 were used in comparison to the recorded abundances by the TIMS. The calculated $^{87}Sr/^{86}Sr$ and $^{143}Nd/^{144}Nd$ isotope ratios (Table 2) and δ^{13}Corg are shown versus stratigraphic height for the Iona-1 core (Figure 3). The shaded region defines the duration of the MCE based on the distinguished double peak positive shift of δ^{13}Corg values relative to the background values. In figure 3, $^{87}Sr/^{86}Sr$ ratios show a positive excursion followed by a negative excursion followed by an additional

positive excursion. These excursions are minor, occurring over relatively short durations (5 to 10 ka) and showing a quick recovery to pre-excursion $^{87}Sr/^{86}Sr$ ratios. Minor excursions of $^{87}Sr/^{86}Sr$ are significant because the long-term ocean residence time of Sr (several million years) is expected to result in less rapid shifts over a short amount of time (Jones and Jenkyns, 2001).

There is a distinguished outlier in the ε Nd data that can be interpreted in one of two ways. Either the outlier is a true data point, and represents a rapid positive shift to more radiogenic ε Nd seawater values, or the outlier is the result of an error in the data collection process. The best way to distinguish the difference is to re-run the Nd and Sm data for this particular sample as well as other samples immediately above and below this sample's stratigraphic height. In figure 3, the first positive shift from -27.88 to -24.98 in δ^{13}Corg represents the onset of the MCE. The ε Nd shows constant values of ~ -3.4 during the pre-MCE interval, and begins to increase rapidly from -4.14 to -0.56 alongside the initial δ^{13}Corg rise. Following this maximum, ε Nd rapidly declines to -2.84 at the same time δ^{13}Corg reaches a minimum following the first maximum. The second δ^{13}Corg maximum corresponds with a minor ε Nd maximum.

Distinct increases in ε Nd values have been theorized to indicate intense submarine volcanism. In figure 3, the positive excursion in $^{187}Os/^{188}Os$ from 0.892 to 1.262 corresponds with the first maximum in δ^{13}Corg. The $^{187}Os/^{188}Os$ positive excursion indicates increased radiogenic input from continental weathering. The positive $^{187}Os/^{188}Os$ excursion occurs shortly after the positive ε Nd excursion (5 Ky) and shows opposing environmental indications. These opposing indications are further investigated in the discussion section of this study. A negative

$^{187}Os/^{188}Os$ excursion occurs after the both of the peaks in $\delta^{13}Corg$ and may indicate a delayed signal of submarine volcanic activity.

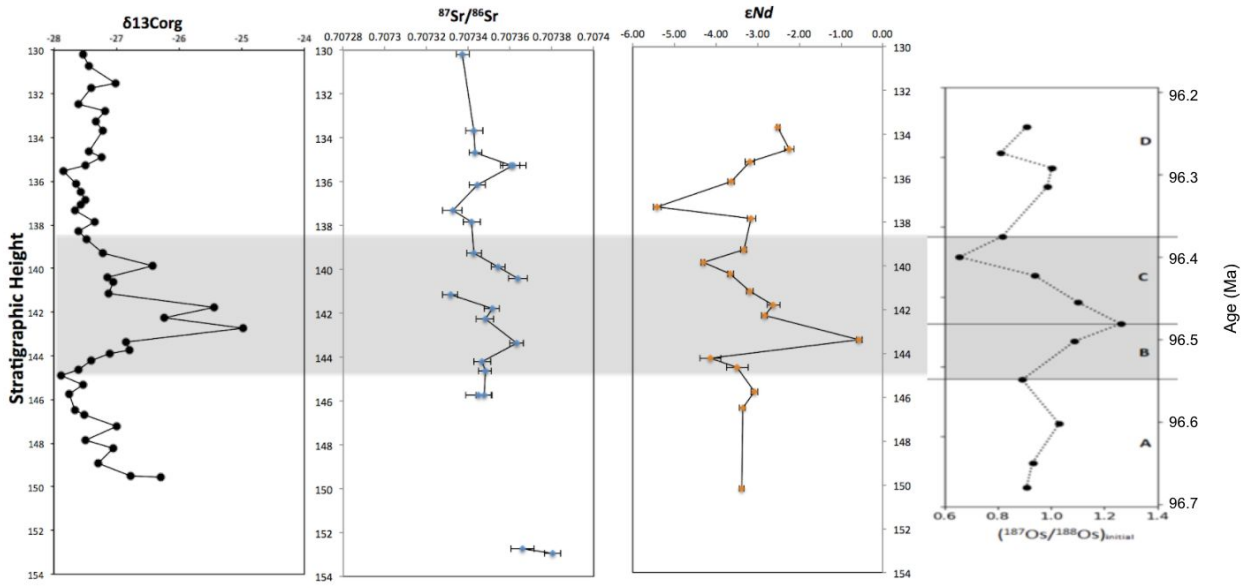

Figure 3: Plot showing δ^{13}Corganic (Eldrett et al., 2014), ε Nd, $^{87}Sr/^{86}Sr$, and $^{187}Os/^{188}Os$ (Lauckner, 2018) for the Iona-1 research core. The grey shading indicates the δ^{13}C excursion that defines the extent of the Mid-Cenomanian Event. See text for discussion.

Sample age (Ma)	Sr (ppb)	Mn (ppb)	Co (ppb)	Cu (ppb)	Zr (ppb)	La (ppb)	Ce (ppb)	Pr (ppb)	Nd (ppb)	Sm (ppb)	Eu (ppb)	Gd (ppb)	Tb (ppb)	Dy (ppb)	Ho (ppb)	Er (ppb)	Tm (ppb)	Yb (ppb)	Lu (ppb)
96.06	999.430	45.746	0.780	3.255	0.091	5.104	6.440	0.682	2.475	0.479	0.116	0.568	0.093	0.620	0.144	0.464	0.073	0.512	0.091
96.11	570.849	89.899	0.123	-0.061	0.232	1.426	1.918	0.227	0.852	0.163	0.046	0.187	0.030	0.177	0.042	0.127	0.022	0.123	0.025
96.14	495.414	112.395	0.072	-0.069	0.071	0.737	0.872	0.108	0.462	0.095	0.027	0.110	0.016	0.084	0.020	0.054	0.009	0.051	0.011
96.19	577.412	26.338	1.447	0.725	0.033	1.767	2.378	0.291	1.172	0.238	0.070	0.252	0.039	0.233	0.052	0.161	0.027	0.195	0.034
96.25	605.161	160.453	0.295	0.101	0.097	1.420	1.650	0.204	0.870	0.181	0.041	0.212	0.034	0.199	0.048	0.145	0.022	0.145	0.028
96.28	51.569	54.685	53.966	54.870	54.400	55.949	55.545	55.606	53.053	53.125	52.484	53.413	54.505	52.277	54.368	52.518	54.051	51.492	55.044
96.35	577.380	30.051	1.027	2.481	0.042	2.931	3.833	0.424	1.570	0.308	0.076	0.341	0.050	0.350	0.080	0.268	0.043	0.327	0.057
96.38	767.543	31.235	2.107	0.243	0.069	3.814	5.712	0.660	2.543	0.501	0.112	0.533	0.080	0.555	0.119	0.379	0.062	0.448	0.074
96.41	697.663	45.093	0.982	0.760	0.063	3.834	5.596	0.665	2.526	0.515	0.121	0.540	0.075	0.500	0.107	0.336	0.052	0.352	0.061
96.45	872.555	36.665	0.972	1.021	0.050	3.820	5.784	0.686	2.558	0.484	0.124	0.497	0.074	0.481	0.104	0.311	0.048	0.344	0.054
96.48	589.451	95.175	0.070	-0.056	0.048	0.885	1.169	0.136	0.559	0.114	0.025	0.126	0.017	0.114	0.025	0.078	0.011	0.077	0.014
96.50	51.569	54.685	53.966	54.870	54.400	55.949	55.545	55.606	53.053	53.125	52.484	53.413	54.505	52.277	54.368	52.518	54.051	51.492	55.044
96.55	926.893	37.815	0.861	3.140	0.051	4.287	5.454	0.612	2.297	0.455	0.111	0.513	0.079	0.546	0.124	0.408	0.063	0.443	0.074
96.59	595.736	100.802	0.121	0.036	0.022	0.312	0.301	0.039	0.180	0.037	0.008	0.051	0.006	0.045	0.009	0.025	0.004	0.027	0.005
96.62	598.358	35.596	0.922	0.494	0.024	2.082	3.001	0.369	1.424	0.284	0.069	0.291	0.043	0.286	0.057	0.187	0.026	0.174	0.030
96.67	758.765	36.194	1.113	3.189	0.028	1.187	1.511	0.192	0.773	0.155	0.045	0.186	0.028	0.190	0.044	0.135	0.021	0.145	0.024
96.70	665.731	35.135	1.284	1.749	0.029	1.717	2.316	2.316	0.285	1.140	0.236	0.054	0.273	0.040	0.277	0.060	0.185	0.028	0.206
96.89	760.688	29.983	1.222	0.189	0.035	3.540	5.551	5.551	0.736	2.804	0.601	0.137	0.656	0.100	0.671	0.146	0.439	0.067	0.465

Table 1: Heavy metal elements and REEs abundances corrected for mass fractionation reported as parts-per-billion (ppb) concentrations.

Sample #	Age	147Sm/144Nd ICPMS	147Sm/144Nd TIMS	143Nd/144Nd	±2σ	143Nd/144Nd Sample@T	εNd today	εNd time	87/86 Sr	±2σ
133.68	96.06	0.1171	0.1189	0.51246052	0.0000027	0.51238578	-3.46	-2.51	0.707343	0.0000042
134.65	96.11	0.1157	0.1147	0.51247189	0.0000054	0.51239976	-3.24	-2.24	0.707343	0.0000033
135.25	96.14	0.1239	0.1197	0.51242633	0.0000054	0.51235107	-4.13	-3.18	0.707361	0.0000040
136.14	96.19	0.1230	0.1201	0.51240341	0.0000039	0.51232785	-4.58	-3.64	0.707344	0.0000039
137.31	96.25	0.1261	0.1243	0.51231546	0.0000043	0.51223718	-6.29	-5.40	0.707332	0.0000046
137.85	96.28	0.1189	0.1136	0.51242426	0.0000055	0.51235269	-4.17	-3.15	0.707342	0.0000041
139.27	96.35	0.1225	0.1198	0.51241836	0.0000038	0.51234285	-4.28	-3.34	0.707343	0.0000034
139.86	96.38	0.1192	0.1182	0.5123674	0.0000020	0.51229284	-5.28	-4.31	0.707354	0.0000035
140.39	96.41	0.1234	0.1196	0.51240231	0.0000036	0.51232686	-4.60	-3.65	0.707364	0.0000046
141.15	96.45	0.1144	0.1417	0.51244036	0.0000044	0.51235092	-3.86	-3.18	0.707372	0.0000072
141.77	96.48	0.1236	0.1201	0.51245523	0.0000082	0.51237941	-3.57	-2.62	0.707351	0.0000035
142.27	96.50	0.1197	0.1202	0.51244413	0.0000036	0.51236823	-3.78	-2.84	0.707348	0.0000041
143.37	96.55	0.1129	0.1097	0.51255445	0.0000033	0.51248518	-1.63	-0.56	0.707363	0.0000034
144.21	96.59	0.1257	0.1289	0.51238307	0.0000130	0.51230163	-4.97	-4.14	0.707347	0.0000041
144.63	96.62	0.1204	0.1220	0.51241234	0.0000130	0.51233522	-4.40	-3.48	0.707348	0.0000031
145.75	96.67	0.1211	0.1242	0.51243468	0.0000044	0.51235613	-3.97	-3.07	0.707348	0.0000037
146.46	96.70	0.1254	0.1298	0.51242319	0.0000031	0.51234108	-4.19	-3.37	0.707362	0.0000043
150.15	96.89	0.1297	0.1261	0.5124196	0.0000030	0.51233968	-4.26	-3.39	0.707389	0.0000062

Table 2: Summary of ε Nd and $^{87}Sr/^{86}Sr$, isotope ratios corrected to initial values.

4. Discussion

4.1 The mid-Cenomanian Glaciation Hypothesis

Evidence from clay assemblages investigated for paleoclimate in the Aquitaine Basin, France, strongly indicate that the Cenomanian climate was hot and humid (Giraud et al., 2013). Additionally, the Cenomanian has been documented as an episode of eustatic sea-level rise, evidenced by $^{187}Os/^{188}Os$ and $^{143}Nd/^{144}Nd$ isotope ratios (Jarvis et al., 2018). Although the entire Cretaceous period is highlighted by a greenhouse climate, the $\delta^{13}C$ and $\delta^{18}O$ isotope records indicate the upper Cretaceous may have been highlighted by glacial-interglacial cycles (Stoll and Schrag, 2000). Chemostratigraphic identification of sea-level regression caused by glaciation includes positive $\delta^{18}O$ excursions (Stoll and Schrag, 2000). Carbonate data from Italy indicate cyclic global cooling and sea-level regression from multiple positive $\delta^{18}O$ excursions throughout the Cenomanian (Stoll and Schrag, 2000). This indication runs counter to the theory that OAEs are associated with periods of hot climates, eustatic sea-level rise, no glaciation and marine regression.

Results from this study disagree with the mid-Cenomanian glaciation hypothesis where there is a relationship between glacial periods and sea-level regression. Early glacial phases are marked by periods of marine regression and are recognized by negative ε Nd excursions (Holmden et al., 2013). These negative excursions are associated with falling sea-levels exposing greater areas of continental crust that can be weathered. Continental crustal runoff into the oceans produces low radiogenic ε Nd values in the associated seawater (MacLeod et al., 2008). In contrast, ε Nd tends to increase in radiogenic values during interglacial stages of marine highstand (Theiling et al., 2012). If the data from this study were to correspond with the positive $\delta^{18}O$ records from Stoll and Schrag (2000), then a negative ε Nd excursion would be predicted on the lower end of the chemostratigraphic column presented in figure 3. However, the lower interval of figure 3 contains relatively stable ε Nd ratios followed by a rapid positive excursion. The ε Nd data presented in this study not only disagrees with low sea-level and glaciation, it suggests the opposite.

Thus the Nd isotope data from this study does not agree with the positive $\delta^{18}O$ excursions recorded by Stoll and Schrag (2000). Despite the dissimilarity, it should be noted that the difference in geography and the distribution of isotope signals throughout the global oceans are not always correlatable (Thomas and Tilgham, 2013). The Cenomanian is well documented as a period of marine transgression, eustatic sea-level rise and epicontinental sea development (Jarvis et al., 2018). However, a study revisiting eustasy throughout the Cretaceous concludes that the true eustatic shift cannot be observed from one single location due to variations in dynamic topography (Haq, 2014). Sea-level measurements from one single location are representative of eurybatic (local/regional) change, not eustatic (Haq, 2014). Therefore, sea-level

rise documented within the KWIS throughout the MCE may not be the same within the Tethyan ocean (Minisinsi et al., 2018). Additionally, the carbonates collected in Italy were significantly closer to the northern polar region and may have experienced different climatic effects than the Eagle Ford formation which existed closer to the equator during the Mid-Cenomanian (Figure 2). Lastly, the Cenomanian occurred over a period of ~7.4 Ma and Milankovitch cycles occur over short time scales of ~20 - 400 ka (Gabdullin et al., 2014). Therefore, Milankovitch cycles such as eccentricity may have resulted in small scale glacial periods at the poles during the Cenomanian.

4.2 The Ocean Circulation Hypothesis

Paleoclimate studies have credited changes in climate to coincide with changes in ocean circulation patterns (Dera et al., 2015). However, few studies have reconstructed paleocirculation patterns of the Late Cretaceous epoch to observe the relationship between changes in paleocirculation, greenhouse climate, and ocean anoxia (Martin et al., 2002). As noted above, Nd isotopes can be used in reconstructing paleocirculation including the origin, strength and flow direction of paleocurrents (Frank, 2002). The ocean residence time of Nd is significantly shorter than the ocean mixing time, therefore the shifting isotope composition of Nd within ancient seafloor deposits is likely a result of paleocirculation changes (Frank, 2002). Strontium is well mixed within the ocean and has a relatively long residence time of several million years, consequently, the resulting isotope composition in seawater is not representative of changes in paleocirculation (Frank, 2002; Jones and Jenkyns, 2001).

Positive and negative ε Nd excursions have been interpreted as changes in ocean circulation patterns (Martin et al., 2012). A positive excursion may be the result of nutrient-rich, radiogenic ε Nd signature bottom waters upwelling to the surface and promoting primary

productivity and eventually initiating local anoxia (Arther and Sageman, 1994). A positive seawater ε Nd shift may also be indicative of warm surface currents from equatorial based oceans moving into the location of study and promoting a warmer climate and primary productivity within the region (Dera et al., 2015). Additionally, shifting ocean circulation may result in a local negative ε Nd excursion from unradiogenic water masses migration (Dera et al., 2015). A negative ε Nd excursion may be an indicator of continental material eroding and depositing into local, low latitude water mass formations (Martin et al., 2012). This indicator is relevant to the carbonates used in this study, which were deposited under a shallow epicontinental seaway.

Unusually low ε Nd background values as seen from Demerara Rise have been interpreted to be the result of warm saline bottom waters (WSBW) originating from shallow epicontinental sea shelves sinking beneath other water masses due to density differences (Martin et al., 2012; Berrocoso et al., 2010). Sinking of WSBW beneath other water masses is hypothesized to contribute to the longevity of OAE2 (500 ka) (Berrocoso et al., 2010; Zheng et al., 2016). This hypothesis is based on WSBW creating a dynamic nutrient trap through a positive feedback loop of nutrient-rich WSBW feeding the surface water mass, and promoting productivity followed by deoxygenation, and the continuation of a greenhouse climate (Berrocoso et al., 2010). Martin et al. (2012) concluded that the positive ε Nd excursion reflects the movement of warm, saline, nutrient rich bottom waters into the study area, however, the source of the nutrient supply was not determined. Therefore, the source of nutrients and radiogenic Nd to the bottom waters could have been submarine volcanism (Zheng et al., 2013).

Data from this study does not include unusually low ε Nd background values, therefore the nutrient trap hypothesis does not correspond with the MCE as it does with OAE2 (Figure 4).

The ε Nd data representing OAE2 from Demerara Rise has a similar pattern to the ε Nd data from this study in terms of positive and negative excursions (Figure 4) (Martin et al., 2012). Martin et al., (2012) determines that the positive shift observed in Demerara Rise data cannot be the result of volcanism and instead indicates a transition from WSBW to ε Nd enriched North Atlantic bottom waters due to changing ocean circulation. The ε Nd data from this study and from Martin et al., (2012) indicates a positive shift in ε Nd values just before the first positive peak in δ^{13}Corg (Figure 4). Martin et. al. (2012) argues that volcanic Nd cannot be transported in oxic bottom waters due to the immediate removal of Nd by precipitation of Fe-Mn oxides. Additionally, the onset of the δ^{13}Corg peak indicates the beginning of bottom water anoxia, therefore the volcanic input marked by the positive ε Nd excursion cannot pre-date the δ^{13}Corg peak (Martin et al., 2012). However, the δ^{13}Corg data used to compare the ε Nd from Demerara Rise is not derived from the same samples but is sourced from older δ^{13}C studies (Martin et al., 2012; Erbacher et al., 2005). Thomas and Tilgham (2013) strongly express the significance of regional triggers for anoxia rather than one single global trigger due to isotope signal variations across different geographic locations. Therefore, the true local δ^{13}Corg peak could have predated the global one. In addition, the rise in δ^{13}Corg indicates the initiation of ocean anoxia at all depths (especially surface waters) and not explicitly anoxia of bottom waters (Zheng et al., 2013). These implications resurface the possibility of radiogenic Nd input from a volcanic source resulting in the high ε Nd values observed at Demerara Rise and the Iona-1 core (Zheng et al., 2013).

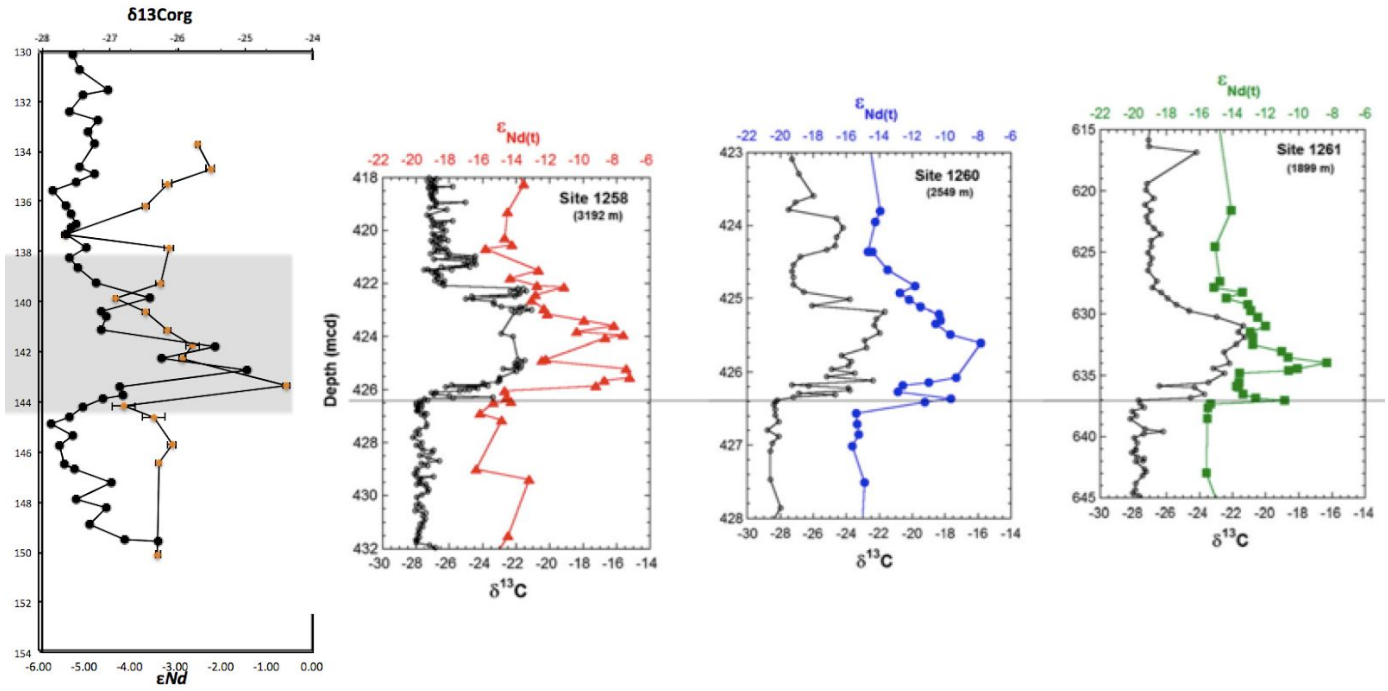

Figure 4: ε Nd data from this study (left figure) compared to ε Nd data encompassing OAE2 from Demerara rise (right three figures) (Martin et al., 2012).

4.3 Emplacement of a Large Igneous Province Hypothesis

Submarine volcanism deposits massive amounts of CO_2 into the oceans and atmosphere, rapidly introducing gigatons of isotopically light carbon into the global carbon cycle, and is theorized to result in an initial negative δ^{13}Corg excursion (Kuroda et al., 2007; Percival et al., 2016). This massive CO_2 input disturbs the carbon cycle and produces a greenhouse climate, setting the stage for ocean anoxia and the subsequent δ^{13}Corg positive excursion associated with enhanced organic carbon burial on the seafloor. If volcanism is involved in the induction of anoxia, then a negative δ^{13}Corg excursion will predate the positive peak in δ^{13}Corg. The δ^{13}Corg data collected by Eldrett et al. (2014) in figure 3 plots a negative excursion just before the following double peak, indicating potential for volcanic involvement in the induction of ocean anoxia. Additionally, a subtle ε Nd negative excursion occurs immediately above the

δ^{13}Corg negative excursion and is likely a result of increased continental weathering associated with the onset of greenhouse climate conditions and beginnings of ocean anoxic conditions (Theiling et al., 2012).

Distinct increases in ε Nd values have been interpreted in geochemical analyses to be the result of submarine volcanism depositing high ε Nd bearing basalts (ε Nd ~ +10) into the ocean basin, leaving a distinct isotopic signal in seawater deposits (MacLeod et al., 2008). The ε Nd values from volcanic sources in the modern oxic ocean is rapidly removed by the precipitation of oxides surrounding the hydrothermal source, however, it is possible that this isotopic signature remains intact if submarine volcanism occurs in an anoxic environment where the precipitation of these oxides is impossible (Frank, 2002; Martin et al., 2012). The ε Nd positive excursion in figure 3 occurs approximately 10 ky before the δ^{13}Corg negative excursion. The emplacement of an LIP may be responsible for the initial negative δ^{13}Corg excursion, followed by massive eruptions depositing radiogenic Nd and producing the later positive ε Nd signal. Additionally, if the ε Nd signal was initially produced by submarine volcanism in a different geographic location than the deposited source rock, the ε Nd signal may appear delayed in time as compared to the δ^{13}Corg signal, as is observed in this data.

If the emplacement of a LIP is responsible for the transition to ocean anoxic conditions, then the ε Nd data is expected to trend towards more radiogenic values, and the $^{187}Os/^{188}Os$ data is expected to trend towards non-radiogenic values (Zheng et al., 2012; Bottini et al., 2012). The ε Nd data from this study does exhibit this positive excursion, however, the $^{187}Os/^{188}Os$ data (Lauckner, 2018) trends towards more radiogenic values (Figure 3). The expected non-radiogenic $^{187}Os/^{188}Os$ signal may have been overprinted by intense local inputs of

continental weathering. This is a reasonable assumption given the hot and humid climate that dominated the MCE in addition to the shallow epicontinental sea depositional environment of the Iona-1 core (Figure 2). There may also be more than one trigger involved in the induction of local anoxia, including both increased continental weathering and submarine volcanism.

If the MCE was triggered by the emplacement of a LIP, then the date of the associated LIP flood basalts must be consistent with the onset of the MCE. There are two potential LIPs that may be responsible for the isotope signals discussed previously, the HALIP, and the CLIP. The lack of available and datable HALIP and CLIP basalt outcrops creates a challenge in crediting LIP involvement with OAEs. Nonetheless, the HALIP has been concluded as a trigger for OAE2 and the early Aptian OAE (OAE 1.a; 120 Ma) (Zheng et al., 2013; Deegan et al., 2016). HALIP basalt production has been described to occur in two pulses, the first dated between 130-120 Ma, and the second pulse between 93-60 Ma (Deegan et al., 2016; Schroder et al., 2019). The first pulse predates the MCE and corresponds with OAE 1.a and the later pulse postdates the MCE and corresponds with OAE2. Estrada et al. (2016) determined a whole rock age of HALIP basalt to be 96.4 ± 1.6 Ma by use of ^{40}Ar -^{39}Aranalysis. If this date is accurate, there is potential for the positive ε Nd excursion to be a result of the HALIP migrating to the Iona-1 via southern moving arctic water masses. However, if the HALIP was responsible for triggering the MCE, then the resulting ε Nd and $^{187}Os/^{188}Os$ signal would likely be delayed and diluted due to the tectonic placement of continental plates (Figure 2). Data from this study does not record this delay, therefore it is suggested here that the emplacement of the HALIP is not represented.

Two studies have dated CLIP igneous activity using ^{40}Ar -^{39}Ar analysis and recovered the following ages; 87 - 95 Ma (Snow et al., 2005) and 98.7 ± 7.7 - 64.5 ± 5 Ma (Serrano et al.,

2011). The later and more recently dated results by Serrano et al. (2011) encompass the MCE. If the CLIP is responsible for the positive ε Nd excursion, water masses would be required to move northward from the CLIP to the Iona-1 location in the KWIS (Figure 2). Eldrett et al. (2017) used total organic carbon (TOC) and major, minor and trace element geochemical analyses to interpret water mass evolution within the KWIS throughout the Late Cretaceous Epoch. Results from Eldrett et al. (2017) conclude that Tethyan water masses moved north into the KWIS from 98-95 Ma. This conclusion corresponds with the proposed timing of CLIP activity by Serrano et al. (2011) and the ε Nd data from this study.

4.4 OAEs: Single Global Trigger, or Multiple Regional Triggers.

Although ε Nd data from the Iona-1 core is consistent with the conclusion that the MCE was triggered by the emplacement of the CLIP, this data was collected from only one location. In addition, the MCE is a notably smaller OAE in terms of the $\delta^{13}C$ excursion being about half that of OAE2 (Zheng et al., 2016). The MCE records a 0.7‰ positive shift in the carbon isotope values whereas OAE2 records a >2‰ positive shift (Coccioni and Galeotti, 2003; Zheng et al., 2016). Given the size of the MCE, it is impractical to assume that one trigger alone produced deoxygenation of the global ocean. The MCE resulted in more regional effects of deoxygenation rather than global, therefore the regional effects may also be the result of regional-scale triggers (Zheng et al., 2016). Consequently, published papers speculating the trigger of the MCE have different results, depending on their geographic location. For example, MCE deposits from the UK revealed a strongly negative ε Nd excursion, deemed to be the result of an increase in the amount of boreal seawater moving into the European epicontinental seaway (Zheng et al., 2016). The negative ε Nd excursion provides evidence for changing ocean circulation affecting the

climate and regional deoxygenation, as opposed to other regions crediting LIPs to the onset of anoxia based on ε Nd positive excursions (Percival et al., 2015). As opposed to a single large-scale trigger, an OAE could be the result of multiple, regional environmental triggers contributing to a global greenhouse climate and enhanced ocean productivity. These individual triggers are ambiguous as they are based on environmental proxies from different isotope data. More regional data constraining the MCE would strengthen this hypothesis.

5. Conclusions

The reconstruction of mid-Cenomanian ε Nd, $^{87}Sr/^{86}Sr$, and $^{187}Os/^{188}Os$ KWIS seawater is presented in this study. The relationship between the positive and negative excursions of ε Nd and δ^{13}Corg corresponds with the timing of the CLIP magmatism and northern flowing ocean circulation patterns in the KWIS. Thus, the highly radiogenic ε Nd signal recovered from the Iona-1 core is a result of the southward emplacement of the CLIP which then migrated northward into the KWIS by way of the northern-flowing equatorial Atlantic Tethyan water mass during the mid-Cenomanian (Serrano et al., 2011; Eldrett et al., 2017). CLIP magmatic activity is therefore at least regionally responsible for the positive δ^{13}Corg excursion defining the onset of the MCE. Increased local continental weathering rates derived by the positive $^{187}Os/^{188}Os$ excursion indicates an additional trigger contributing to ocean anoxic conditions.

Acknowledgments

I would like to extend a special thanks to my advisor, Dr. Alan Brandon for his helpful insight and thought provoking conversations in addition to allowing my use of his radiogenic isotope laboratory and clean laboratory. I would also like to thank Lucien Nana Yobo for

introducing me to the realm of geochemical research and for his patience with me in the lab.

Lastly, I would like to thank my thesis readers Dr. Qi Fu and Dr. Shuhab Khan for their time.

References Cited

Abbott, A.N., Haley, B.A., Tripati, A.K., and Frank, M., 2016, Constraints on ocean circulation at the Paleocene-Eocene Thermal Maximum from neodymium isotopes: Climate of the Past, v. 12, p. 837–847.

Arthur, M., and Sageman, B.B., 1994, Marine Shales: Depositional Mechanisms and Environments of Ancient Deposits: Annual Review of Earth and Planetary Sciences, p. 22, v. 499–551.

Berrocoso, Á.J., MacLeod, K.G., Martin, E.E., Bourbon, E., Londoño, C.I., and Basak, C., 2010, Nutrient trap for Late Cretaceous organic-rich black shales in the tropical North Atlantic: Geology, v. 38, p. 1111–1114.

Blättler, C.L., Jenkyns, H.C., Reynard, L.M., and Henderson, G.M., 2011, Significant increases in global weathering during Oceanic Anoxic Events 1a and 2 indicated by calcium Isotopes. Earth and Planetary Science Letters, v. 309, p. 77–88.

Bottini, C., Cohen, A.S., Erba, E., Jenkyns, H.C., and Coe, A.L., 2012, Osmium-isotope evidence for volcanism, weathering, and ocean mixing during the early Aptian OAE 1a: Geology, v. 40, p. 583–586.

Coccioni, R., and Galeotti, S. 2003, The mid-Cenomanian Event: prelude to OAE 2: Palaeogeography, Palaeoclimatology, Palaeoecology. v. 190, p. 427-440.

Coffin, M.F., and Eldholm, O., 1994, Large igneous provinces: Crustal structure, dimensions, and
external consequences: Reviews of Geophysics. v. 32, p. 1-36.

Deegan, F.M., Troll, V.R., Bédard, J.H., Evenchick, C.A., Dewing, K., Grasby, S., Geiger, H., Freda, C., Misiti, V., and Mollo, S., 2016, The stiff upper LIP. Investigating the High Arctic Large Igneous Province: Geology Today, v. 32, p. 92–98.

Dera, G. et al., 2015, Nd isotope constraints on ocean circulation, paleoclimate, and continental drainage during the Jurassic breakup of Pangea: Gondwana Research. v . 27, p. 1599–1615.

Eldrett, J.S., Ma, C., Bergman, S.C., Lutz,B., Gregory, F.J., Dodsworth, P., Phipps, M., Hardas, P., Minisini, D., Ozkan, A. et.al. 2015, An astronomically calibrated stratigraphy of the Cenomanian, Turonian and earliest Coniacian from the Cretaceous Western Interior Seaway, USA: Implications for global chronostratigraphy: Cretaceous research, v. 56, p. 316-344.

Eldrett, J.S., Dodsworth, P., Bergman, S.C., Wright, M., and Minisini, D. 2017, Water-mass evolution in the Cretaceous Western Interior Seaway of North America and equatorial Atlantic: Climate of the Past, v. 13, p. 855-878.

Eldrett, J.S., Minisini, D., and Bergman, S.C., 2014, Decoupling of the carbon cycle during ocean anoxic event 2: Geology, v. 42, p. 567–570.

Erbacher, J., Friedrich, O., Wilson, P.A., Birch, H., and Mutterlose, J., 2005, Stable organic carbon isotope stratigraphy across Oceanic Anoxic Event 2 of Demerara Rise, western tropical Atlantic: Geochemistry, Geophysics, Geosystems, v. 6, p. 1–9.

Frank, M., 2002, Radiogenic isotopes: Tracers of past ocean circulation and erosional input: Reviews of Geophysics, v. 40, p. 1-38.

Friedrich, O., Erbacher, J., Wilson, P.A., Moriya, K., and Mutterlose, J. 2009, Paleoenvironmental changes across the Mid Cenomanian Event in the tropical Atlantic

Ocean (Demerara Rise, ODP leg 207) inferred from benthic foraminiferal assemblages: Marine Micropaleontology, v. 71, p. 28-40.

Gabdullin, R.R., Samarin, E.N., Ivanov, A. V., Hramov, A.E., Koronovskii, A.A., Runnova, A.E., Yashkov, I.Y., Badulina, N. V., and Igtisamov, D. V., 2014, Astronomo-climatic cycles in the sequence of Upper Cretaceous sediments of the Saratov Volga Region: Moscow University Geology Bulletin, v. 69, p. 323–340.

Giraud, F., Reboulet, S., Deconinck, J.F., Martinez, M., Carpentier, A., and Bréziat, C., 2013, The Mid- Cenomanian Event in southeastern France: Evidence from paleontological and clay mineralogical data: Cretaceous Research, v. 46, p. 43-59.

Halliday, A.N., Davidson, J.P., Holden, P., Owen, R.M., and Olivarez, A.M., 1992, Metalliferous sediments and the scavenging residence time of Nd near hydrothermal vents: Geophys. Res. Lett. v. 19, p. 761–764.

Haq, B.U., 2014, Cretaceous eustasy revisited: Global and Planetary Change, v. 113, p. 44–58

Holmden, C., Mitchell, C., Laporte, D., Patterson, W., Melchin, M., and Finney, S. 2014, Nd isotope records of late Ordovician sea-level change—Implications for glaciation frequency and global stratigraphic correlation: Palaeogeography, Palaeoclimatology, Palaeoecology, v. 386, p. 131–144.

Jarvis, I., Sascha, R.-E., and Selby, D., 2018, Linking sea level, climate, and palaeocirculation change during Mid-Cenomanian Event I (MCE I, 96 Ma): elemental and osmium isotope evidence from southern England: European Geosciences Union General Assembly, 20th, Vienna, Austria, p. 7132.

Kuroda, J., Ogawa, N.O., Tanimizu, M., Coffin, M.F., Tokuyama, H., Kitazato, H., and Ohkouchi, N., 2007, Contemporaneous massive subaerial volcanism and late cretaceous Oceanic Anoxic Event 2: Earth and Planetary Science Letters, v. 256, p. 211–223.

Lauckner, L., 2018, THE UNEXPECTED 187Os/188Os RESPONSE TO THE MID-CENOMANIAN EVENT: AN INVESTIGATION IN THE IONA-1 CORE [Senior thesis]: Houston, University of Houston, 24 p.

MacLeod, K.G., Martin, E.E., and Blair, S.W., 2008, Nd isotopic excursion across Cretaceous ocean anoxic event 2 (Cenomanian-Turonian) in the tropical North Atlantic: Geology, v. 36, p. 811–814.

McLeod, C.L., Brandon, A.D., and Armytage, R.M.G., 2014, Constraints on the formation age and evolution of the Moon from 142Nd-143Nd systematics of Apollo 12 basalts: Earth and Planetary Science Letters, v. 396, p. 179–189.

Martin, E.E., MacLeod, K.G., Berrocoso, A.J., and Bourbon, E. 2012, Water mass circulation on Demerara Rise during the Late Cretaceous based on Nd isotopes. Earth and Planetary Science Letters, 327-328, 111-120.

Minisinsi, D., Eldrett, J., Bergman, S., and Forkner, R. 2018, Chronostratigraphic framework and depositional environments in the organic-rich, mudstone - dominated Eagle Ford Group, Texas, USA: Sedimentology, v. 65, p. 1520-1557.

Moiroud, M., Pucéat, E., Donnadieu, Y., Bayon, G., Guiraud, M., Voigt, S., Deconinck, J.F., and Monna, F., 2016, Evolution of neodymium isotopic signature of seawater during the Late Cretaceous. Implications for intermediate and deep circulation: Gondwana Research, v. 36, p. 503–522.

Percival, L.M.E., Witt, M.L.I., Mather, T.A., Hermoso, M., Jenkyns, H.C., Hesselbo, S.P., Al-Suwaidi, A.H., Storm, M.S., Xu, W., and Ruhl, M., 2015, Globally enhanced mercury deposition during the end-Pliensbachian extinction and Toarcian OAE. A link to the Karoo-Ferrar Large Igneous Province: Earth and Planetary Science Letters, v. 428, p. 267–280.

Percival, L.M.E., Cohen, A.S., Davies, M.K., Dickson, A.J., Hesselbo, S.P., Jenkyns, H.C., Leng, M.J., Mather, T.A., Storm, M.S., and Xu, W., 2016, Osmium isotope evidence for two pulses of increased continental weathering linked to Early Jurassic volcanism and climate Change: Geology, v. 44, p. 759–762.

Jenkyns, H.C., 2010, Geochemistry of ocean anoxic events: Geochemistry, Geophysics, Geosystems, v. 11, p. 1-30.

Jones, Charles E. and Jenkyns, Hugh C. 2001, Seawater strontium isotopes, oceanic anoxic events, and seafloor hydrothermal activity in the Jurassic and Cretaceous: American Journal of Science, v. 2, p. 112-149.

Serrano, L., Ferrari, L., Martínez, M., Petrone, C., & Jaramillo, C. 2011, An integrative geologic, geochronologic and geochemical study of Gorgona Island, Colombia: Implications for the formation of the Caribbean Large Igneous Province: Earth and Planetary Science Letters, 309(3), 324–336.

Sun, X., Zhang, T., Sun, Y., Milliken, K.L., and Sun, D. 2016, Geochemical evidence of organic matter source input and depositional environments in the lower and upper Eagle Ford Formation, south Texas: Organic Geochemistry, v. 98.

Stoll, H., and Schrag, D. 2000. High-resolution stable isotope records from the Upper Cretaceous rocks of Italy and Spain: Glacial episodes in a greenhouse planet? Geological Society of America. v. 112(2), p.308–319.

Theiling, B.P., Elrick, M., and Asmerom, Y., 2012, Increased continental weathering flux during orbital-scale sea-level highstands: Evidence from Nd and O isotope trends in Middle Pennsylvanian cyclic carbonates: Palaeogeography, Palaeoclimatology, Palaeoecology, v. 343, p. 17–26.

Thomas, D. J. and Tilghman, D. S. 2014, Geographically different oceanographic responses to global warming during the Cenomanian-Turonian interval and Oceanic Anoxic Event 2: Palaeogeography, Palaeoclimatology, Palaeoecology. v. 411, p. 136–143.

Van De Flierdt, T., Grifths, A.M., Lambelet, M., Little, S.H., Stichel, T., and Wilson, D.J., 2016, Neodymium in the oceans: A global database, a regional comparison and implications for palaeoceanographic research. Philosophical Transactions of the Royal Society A: Mathematical, Physical and Engineering Sciences, v. 374.

Wright, Z.A., Quinton, P.C., Martin, E.E., Leslie, S.A., MacLeod, K.G., and Herrmann, A.D. 2017, Neodymium isotope ratios and a positive d13C excursion: interpreting the connection between oceanographic and climate changes during the early Late Ordovician of Laurentia: Stratigraphy, v. 14, p. 443-456.

Zheng, X.Y., Jenkyns, H.C., Gale, A.S., Ward, D.J., and Henderson, G.M. 2013, Changing ocean circulation and hydrothermal inputs during Ocean Anoxic Event 2 (Cenomanian-Turonian): Evidence from Nd-isotopes in the European shelf sea: Earth and Planetary Science Letters, v. 375, p. 338-348.